Finite Element Model for Hysteretic Friction Damping of Traveling Wave Vibration in Axisymmetric Structures

X. W. Tangpong
Mem. ASME
Department of Mechanical Engineering and Applied Mechanics,
North Dakota State University,
Fargo, ND 58105

J. A. Wickert[1]
Fellow ASME
Department of Mechanical Engineering,
Iowa State University,
Ames, Iowa 50011
e-mail: wickert@isu.edu

A. Akay
Fellow ASME
Department of Mechanical Engineering,
Carnegie Mellon University,
Pittsburgh, PA 15213

A finite element method is developed to treat the steady-state vibration of two axisymmetric structures—a base substructure and an attached damper substructure—that are driven by traveling wave excitation and that couple through a spatially distributed hysteretic friction interface. The base substructure is representative of a rotating brake rotor or gear, and the damper is a ring affixed to the base under preload and intended to control vibration through friction along the interface. In the axisymmetric approximation, the equation of motion of each substructure is reduced in order to the number of nodal degrees of freedom through the use of a propagation constant phase shift. Despite nonlinearity and with contact occurring at an arbitrarily large number of nodal points, the response during sticking, or during a combination of sticking and slipping motions, can be determined from a low-order set of computationally tractable nonlinear algebraic equations. The method is applicable to element types for longitudinal and bending vibration, and to an arbitrary number of nodal degrees of freedom in each substructure. In two examples, friction damping of the coupled base and damper is examined in the context of in-plane circumferential vibration (in which case the system is modeled as two unwrapped rods), and of out-of-plane vibration (alternatively, two unwrapped beams). The damper performs most effectively when its natural frequency is well below the base's natural frequency (in the absence of contact), and also when its natural frequency is well separated from the excitation frequency. [DOI: 10.1115/1.2775519]

Keywords: friction-vibration interaction, hysteretic damping, axisymmetric structures, propagation constant

1 Introduction

Friction damping can be a useful and practical means to passively control mechanical vibration, particularly in rotating machinery or high-temperature applications. In one embodiment, a damper is attached to a vibrating base structure, and vibration energy is dissipated through the friction and relative motion between the two systems. Such dampers can contact the base structure at discrete points, as in gas turbine blades, or along a spatially distributed interface. Figure 1 depicts a ring damper that is affixed to the outer periphery of a ventilated automotive brake rotor in a groove machined within the cooling vanes. Vibration of the rotor that develops during braking couples with the dynamics of the ring damper through the friction interface, and undesirable vibration of the rotor can be attenuated [1]. Ring dampers can be affixed to ventilated or nonventilated rotors, or placed at the rotor's inner or outer peripheries [2], in order to reduce squeal noise. Ring dampers can also be used to control vibration of automotive brake drums [3].

In those applications, the ring damper is capable of introducing significant dissipation to the brake rotor or drum, as compared to otherwise identical components alone. The bending vibration of the combined rotor and ring damper system, and of an identical brake rotor alone, were measured through standard modal testing procedures using an impact hammer and accelerometer (PCB Instruments). In each measurement of the rotor's transverse bending vibration, the accelerometer was located on the inner cheek's surface near the rotor's periphery. In Fig. 2, the ring damper is shown to reduce the rotor's amplitude by an average of 88% in the first eight modes within the frequency range 1.2–13.6 kHz.

The level of dissipation afforded by a friction damper can be tuned and optimized by adjusting the interfacial preload between a damper and its base structure [4–8]. When the preload is too small, little energy is dissipated owing to the friction force's small magnitude. Likewise, when the preload is too large, little dissipation again develops because the interface locks up with insufficient slippage between the two systems. Other design variables, such as the mass and natural frequency ratios between the base and the damper, also influence the damper's effectiveness. With application to ring dampers used to control vibration of highly loaded gears, for instance, an empirical relation between the damper's and the gear's weights was offered without derivation in [9]. For distributed contact friction dampers, in particular, the tuning of the design variables to maximize dissipation is often achieved through repeated fabrication and testing, or through approximate models. In [10], a friction damper for controlling vibration in a high-speed printer was modeled as an infinitely long beam subjected to periodic impact loads. That analysis, however, was approximate in the sense that it ignored dynamic coupling between the damper and its base structure, and it did not consider the spatial distribution of friction along the interface. In an investigation of split ring dampers used for air seals in a jet engine's compressor [11], the response of the base structure and damper was treated by a static deformation model.

Ring dampers can be treated as a beam having either free boundary conditions (as is representative of a split snap ring) or periodic boundary conditions (a continuous ring) [8]. As an analog

[1]Corresponding author.

Contributed by the Technical Committee on Vibration and Sound of ASME for publication in the JOURNAL OF VIBRATION AND ACOUSTICS. Manuscript received December 29, 2006; final manuscript received May 22, 2007; published online November 12, 2007. Review conducted by Jean Zu.

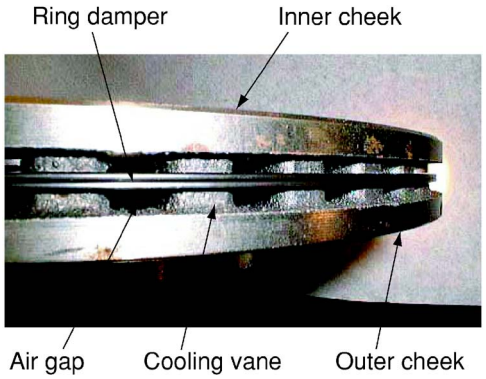

Fig. 1 Side view of an automotive disk brake rotor. The ring damper is affixed to the rotor's periphery in a groove that is machined across the rotor's pattern of cooling vanes.

for circumferential vibration of an "unwrapped" ring and disk, the ring damper assembly was modeled in [4] as a serial connection of spring-mass oscillators that couple in longitudinal vibration through pointwise hysteretic friction. When the damper is significantly lighter than the base and the excitation frequency is well separated from the base's natural frequency in the absence of contact, a simpler model that accounts only for coupling from the base structure to the damper provides a good approximation to the fully coupled system's response.

Vibration of brake rotors and drums, bladed turbine disks, and gears is often excited by forces that are applied in a stationary reference frame. In the structure's (rotating) frame, the excitation takes the form of a periodic moving load that generates traveling wave response in an axisymmetric structure [12]. In the simplest case, and in what follows, the traveling wave excitation and the response are represented by the first term of Fourier expansions. When an axisymmetric structure is undergoing traveling wave vibration, the vibration amplitude remains the same from one location to another, but a phase shift is present between locations. An

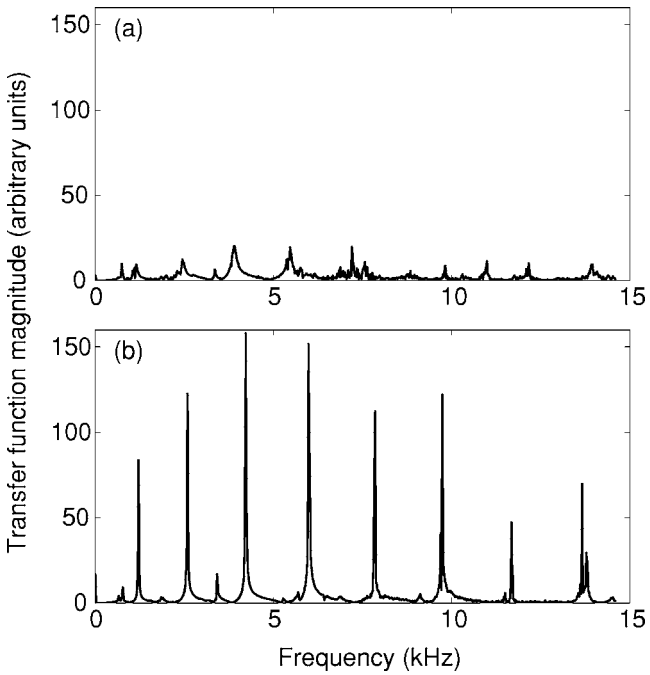

Fig. 2 Measured collocated point frequency response functions for (*a*) an automotive brake rotor that incorporates a ring damper, as in Fig. 1, and (*b*) an otherwise identical rotor alone

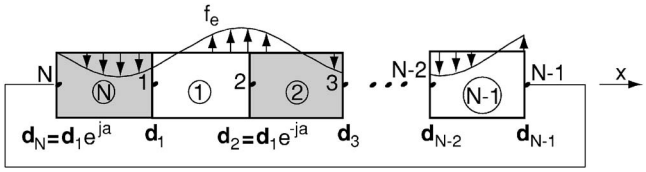

Fig. 3 Nomenclature and illustration of the geometry for adjoining elements in a structure that has periodic boundary conditions and is excited by traveling wave vibration

imaginary phase constant can be introduced to correlate responses at two spatially separated locations in a manner analogous to the propagation constant as employed in the treatment of traveling wave vibration in periodic structures [13,14].

This paper describes a finite element method that can be used to obtain the steady-state traveling wave response of two axisymmetric structures that couple through distributed friction damping. The motivation for the model is the application of ring dampers to rotating base structures including drums, disks, rotors, gears, and other machine components. Owing to axisymmetry and the particular form of traveling wave excitation that is chosen, the system's response can be obtained by analyzing only one element of each substructure, regardless of the number of elements used in discretization. Furthermore, despite nonlinearity in which the interface is characterized by hysteretic friction, and with contact occurring at an arbitrarily large number of points, the response during sticking, or during a combination of sticking and slipping motions, can be determined from a low-order set of computationally tractable algebraic equations. In the first example, the model is applied to treat the friction damping of longitudinal traveling wave vibration in two rods, and the resulting governing equations are shown to be identical to those obtained from the alternative discrete model in [4]. The method is then used to examine friction damping of traveling wave bending vibration in two hysteretically coupled beams.

2 Finite Element Model

Figure 3 depicts adjoining elements in a closed axisymmetric structure having periodic boundary conditions. The structure is subjected to traveling wave excitation of the form

$$f_e = f_0 e^{j(\omega t - 2\pi n x/L)} \tag{1}$$

where $j=\sqrt{-1}$, f_0 is the magnitude of the applied force per unit of length, ω is the excitation frequency, n is the spatial wave number, and L is the structure's length or circumference. The excitation and the structure's ensuing steady-state traveling wave response can be oriented either in the structure's plane or normal to it. The degree of freedom and the number N of elements in Fig. 3 are arbitrary. Since the excitation at location x_i, with $i=1,2,\ldots,N$, has the same magnitude as the excitation at $x_1=0$, but for the phase delay $2\pi n x_i/L$, the structure's steady-state response at x_i likewise is shifted in phase relative to the response at the first node [15]. The vector of generalized nodal coordinates at point i, representing physical displacements and rotations, is related to the coordinates at the first node by[2]

$$\mathbf{d}_i = \mathbf{d}_1 e^{-ja(i-1)} \tag{2}$$

where the propagation constant is defined $a=2\pi n/N$. For an axisymmetric structure, the propagation constant satisfies [14]

$$e^{-jaN} = 1 \tag{3}$$

and the coordinate vector at node N becomes

[2]Symbols in bold denote matrices or vectors.

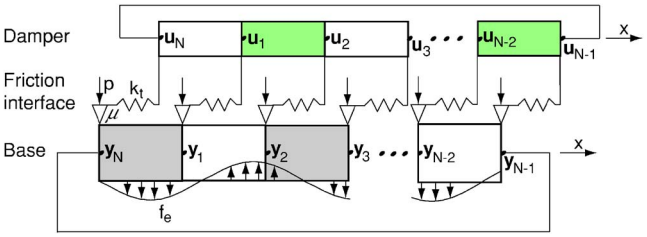

Fig. 4 Nomenclature and illustration of the geometry for two structures, each having periodic boundary conditions, that couple through a spatially distributed friction interface. The base structure is excited by traveling wave excitation.

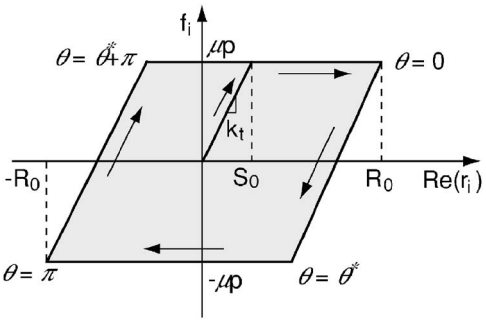

Fig. 5 Bilinear hysteresis response at the *i*-th contact element within the interface

$$\mathbf{d}_N = \mathbf{d}_1 e^{-ja(N-1)} = \mathbf{d}_1 e^{ja} \tag{4}$$

When the structure is partitioned into n contiguous sectors, each responds with identical amplitude, but with phase shifts between each station. In particular, the coordinates associated with nodes 2 and N couple and contribute to the response at the structure's first node. Since the responses at nodes 1, 2, and N couple through the complex phase shift expressions, by using Eq. (2), the degree of freedom in the model can be reduced to that for a single node.

For the first and last elements, the elemental stiffness and mass matrices are given generally by

$$\mathbf{K}^{e(1)} = \begin{matrix} \mathbf{d}_1 & \mathbf{d}_2 \\ \end{matrix} \begin{bmatrix} \mathbf{K}_{11} & \mathbf{K}_{12} \\ \mathbf{K}_{21} & \mathbf{K}_{22} \end{bmatrix} \begin{matrix} \mathbf{d}_1 \\ \mathbf{d}_2 \end{matrix} \quad \text{and} \quad \mathbf{K}^{e(N)} = \begin{matrix} \mathbf{d}_N & \mathbf{d}_1 \\ \end{matrix} \begin{bmatrix} \mathbf{K}_{11} & \mathbf{K}_{12} \\ \mathbf{K}_{21} & \mathbf{K}_{22} \end{bmatrix} \begin{matrix} \mathbf{d}_N \\ \mathbf{d}_1 \end{matrix} \tag{5}$$

where the vectors $\mathbf{d}_i$ placed outside of each matrix represent the coordinates corresponding to the block elements of the matrices. Each block $\mathbf{K}_{ik}$ ($i, k=1$ or 2) has J degrees of freedom. In the light of Eq. (2), the global g stiffness matrix that corresponds to $\mathbf{d}_1$ is

$$\mathbf{K}_1^g = \mathbf{K}_{11} + \mathbf{K}_{22} + \mathbf{K}_{12} e^{-ja} + \mathbf{K}_{21} e^{ja} \tag{6}$$

where the phase factors $e^{\pm ja}$ are associated with coordinates $\mathbf{d}_2$ and $\mathbf{d}_N$. The global mass matrix for $\mathbf{d}_1$ is constructed analogously. In this manner, the degree of freedom in the structural model is reduced from NJ to J.

When two such axisymmetric structures couple through distributed frictional contact, they can be represented as in Fig. 4. The base structure is subjected to a traveling wave force of the form (1), and the two structures contact at N nodal locations. The local friction force is modeled in the hysteretic sense by a serial connection of tangential stiffness k_t and friction under preload p. The orientations of excitation f_e and preload p in Fig. 4 are shown for illustrative purposes, as the excitation can be directed in or out of the base's plane. The friction force is parametrized by

$$k_t = \frac{k_F}{N} \quad \text{and} \quad p = \frac{p_0 L}{N} \tag{7}$$

where k_F is the tangential stiffness of the entire interface and p_0 is the normal preload force per unit of length. Parameter μ in Fig. 4 denotes the coefficient of friction.

For a coupled base/damper system, the model's degree of freedom can be reduced by using the phase shift constraint. The responses at the first nodes of each structure satisfy

$$\mathbf{M}_B \ddot{\mathbf{y}} + \mathbf{C}_B \dot{\mathbf{y}} + \mathbf{K}_B \mathbf{y} = \mathbf{F}_E + \mathbf{F}_f \tag{8}$$

$$\mathbf{M}_D \ddot{\mathbf{u}} + \mathbf{C}_D \dot{\mathbf{y}} + \mathbf{K}_D \mathbf{y} = -\mathbf{F}_f \tag{9}$$

where the subscripts B and D denote the base and the damper, respectively, and all matrices are developed as in Eq. (6). Nodes within the base structure and the damper can have different degrees of freedom. Vectors $\mathbf{y}$ and $\mathbf{u}$ represent the generalized coordinates for responses at the first nodes in each case. The excitation $\mathbf{F}_E$ and friction $\mathbf{F}_f$ forces are applied to the base's first node. Under the traveling wave excitation of Eq. (1),

$$\mathbf{y} = \mathbf{y}_a e^{j(\omega t - \beta)} \quad \text{and} \quad \mathbf{u} = \mathbf{u}_a e^{j(\omega t - \alpha)} \tag{10}$$

where $\mathbf{y}_a$ and $\mathbf{u}_a$ represent the amplitudes, and β and α are the distinct phase differences between the base's and the damper's responses relative to f_e.

3 Sticking and Sticking/Slipping Phases

The friction force vector $\mathbf{F}_f$ has nonzero elements only at the degrees of freedom for which the base and damper couple, and the friction force assumes different functional forms when the interface experiences pure sticking motion, or a combination of sticking and slipping. The type of interfacial response is determined from the relative displacement

$$\mathbf{r} = \mathbf{u} - \mathbf{y} = \mathbf{r}_a e^{j(\omega t - \psi)} \tag{11}$$

of amplitude $\mathbf{r}_a$ and phase ψ. When the base and damper couple in the qth degree of freedom, the relative motion becomes

$$r_q = R_0 e^{j(\omega t - \psi)} \tag{12}$$

which is also the qth element of vector $\mathbf{r}$ in Eq. (11). The friction force f_q developed at the first node's interface changes with r_q in a manner depicted by the bilinear hysteresis loop in Fig. 5. Parameter S_0 in Fig. 5 denotes the relative displacement at which slipping commences, and it is given by

$$S_0 = \frac{\mu p}{k_t} = \frac{\mu p_0 L}{k_F} \tag{13}$$

When the interface is in its sticking phase, $R_0 \leq S_0$, and the friction force applied to the base structure's first node becomes

$$f_q = k_t (u_q - y_q) \tag{14}$$

where

$$u_q = U_0 e^{j(\omega t - \alpha)} \quad \text{and} \quad y_q = Y_0 e^{j(\omega t - \beta)} \tag{15}$$

are the qth elements of $\mathbf{u}$ and $\mathbf{y}$, respectively. The response amplitudes U_0 and Y_0, and phases α and β, are determined subsequently by balancing the coefficients of $e^{j\omega t}$ in Eqs. (8) and (9).

When relative slipping does occur, the harmonic balance method is an efficient means for representing the nonlinear friction force that develops in the steady state [4,5,16]. This approximate analytical procedure is useful to the extent that direct numerical simulation of transient hysteretic frictional response can be computationally expensive, even when only a single hysteretic element is present [17,18]. In that case, the relative displacement and velocity must be tracked at each time step and at each contact point in order to locate the locations and transitions in state between slipping and sticking. For a system having a large number of hysteretic elements (such as the one depicted in Fig. 4), direct integration becomes prohibitive in the light of the multiplicity of possible states at each time step. The traveling wave excitation

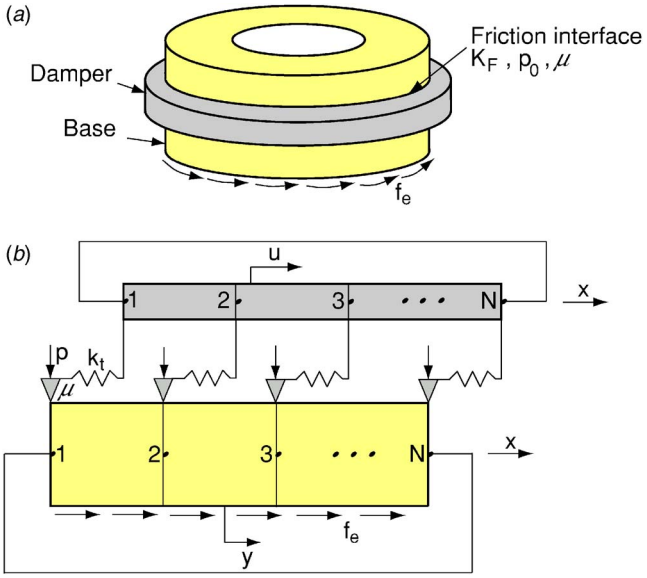

Fig. 6 (*a*) Base structure and ring damper systems that are subjected to circumferential traveling wave excitation and (*b*) an idealized model comprising two unwrapped rods that have periodic boundary conditions and that couple through a spatially distributed friction interface

and axisymmetry of the structures in the present case render an analytical solution possible, which can serve also as a point of comparison for the development of computational methods for frictionally coupled vibration problems.

In a first-term harmonic approximation, the friction force applied to the base's first node is given by

$$f_q \approx \tilde{f}_q = f_c \cos\theta + f_s \sin\theta \tag{16}$$

where $\theta = \omega t - \psi$. Angle $\theta^* = \cos^{-1}(1 - 2S_0/R_0)$ in Fig. 5 demarcates the transition from sticking to slipping over one-half cycle of response. The Fourier coefficients of $\tilde{f}_q$ are determined from

$$f_c = \frac{2}{\pi}\int_0^\pi f_q \cos\theta d\theta \quad \text{and} \quad f_s = \frac{2}{\pi}\int_0^\pi f_q \sin\theta d\theta \tag{17}$$

The Fourier expansion of $\tilde{f}_q$ can be further expressed in its complex form

$$\tilde{f}_q = f_{c1} e^{j\theta} + f_{-c1} e^{-j\theta} \tag{18}$$

where $f_{c1} = (f_c - j f_s)/2$, and $f_{-c1} = (f_c + j f_s)/2$. The desired relation that governs the response of the system's relative motion amplitude R_0 is obtained by balancing the coefficients of $e^{j\theta}$ and of $e^{-j\theta}$ in Eqs. (8) and (9).

4 Friction Damping of Longitudinal Vibration

Figure 6(*a*) illustrates application of the finite element method to a base structure that is driven in its circumferential direction and that couples with the ring damper's vibration through friction. The base and damper are considered to be "unwrapped" rods that vibrate only in the longitudinal direction as in Fig. 6(*b*). The rods contact each other at N locations with hysteretic parameters, as indicated in Fig. 4. The nodal coordinate vectors $\mathbf{y}$ and $\mathbf{u}$ each have only a single element, and they are given by Eq. (15). The system is modeled as two continuous rods that are discretized through the finite element approach of Eqs. (8) and (9). The model is nondimensionalized in terms of the quantities

$$K^* = \frac{k_B}{k_D}, \quad M^* = \frac{m_B}{m_D}, \quad K_{\mathrm{FD}} = \frac{k_F}{k_D}, \quad F = \frac{f_0}{k_B}, \quad P = \frac{\mu p_0}{k_B}$$

$$t^* = \frac{t}{2\pi/\Omega_D}, \quad \eta = \frac{\omega}{\Omega_D}, \quad Y = \frac{Y_0}{L}, \quad U = \frac{U_0}{L}, \quad R = \frac{R_0}{L}, \quad S = \frac{S_0}{L} \tag{19}$$

where $k_{B(D)}$ denotes the axial stiffness of the base (or damper) rod, $m_{B(D)}$ is the mass of the base (or damper) rod, and $\Omega_D = 2\pi\sqrt{k_D/m_D}$ denotes the first flexible body natural frequency of the damper in the absence of contact with the base. The ratio of natural frequencies between the base and the damper (in the absence of contact) is denoted $\gamma = \sqrt{K^*/M^*}$.

The elemental mass and stiffness matrices for the one-dimensional base rod are

$$\mathbf{M}^e = \begin{bmatrix} 2 & 1 \\ 1 & 2 \end{bmatrix} \frac{M^* L_e}{6} \quad \text{and} \quad \mathbf{K}^e = \begin{bmatrix} 1 & -1 \\ -1 & 1 \end{bmatrix} \frac{K^*}{L_e} \tag{20}$$

where the elemental length is denoted $L_e = 1/N$. For the ith element of the base, the generalized force vector is

$$\mathbf{F}^e = e^{j[\omega^* t^* - a(i-1)]} \left(\frac{f_0 N}{4\pi^2 n^2}\right) \begin{Bmatrix} -e^{-ja} - ja + 1 \\ e^{-ja}(ja+1) - 1 \end{Bmatrix} \tag{21}$$

in terms of the propagation constant and $\omega^* = 2\pi\eta$. Following Eq. (6), the global mass and stiffness matrices, and the excitation vector, reduce to the scalar quantities

$$M_B = \frac{M^*}{6N}\left[2 + 4\cos^2\left(\frac{\pi n}{N}\right)\right] \approx \frac{M^*}{N} \tag{22}$$

$$K_B = 4K^* N \sin^2\left(\frac{\pi n}{N}\right) \approx \frac{4K^* \pi^2 n^2}{N} \tag{23}$$

$$F_E = FK^* e^{j\omega^* t^*} \left(\frac{N}{\pi^2 n^2}\right) \sin^2\left(\frac{\pi n}{N}\right) \approx \frac{FK^*}{N} e^{j\omega^* t^*} \tag{24}$$

where the approximations are made as the number of elements in the model is increased, namely, as $N/n \to \infty$. Similarly, the mass and stiffness matrices for the damper's rod become

$$M_D = \frac{M_B}{M^*} \quad \text{and} \quad K_D = \frac{K_B}{K^*} \tag{25}$$

When the interface sticks, the interfacial force applied to the first node of the base depends only on stiffness, and the normalized friction force is

$$F_f = \frac{K_{\mathrm{FD}}}{N}(u_q^* - y_q^*) \tag{26}$$

where $u_q^* = u_q/L$, $y_q^* = y_q/L$, and u_q and y_q are given by Eq. (15). By substituting Eqs. (22)–(26) into Eqs. (8) and (9), the base and damper's responses are determined from the simultaneous solution of

$$(D_1 + 1) Y \cos(\omega^* t^* - \beta) - D_2 Y \sin(\omega^* t^* - \beta) = \frac{FK^*}{K_{\mathrm{FD}}} \cos(\omega^* t^*) + U \cos(\omega^* t^* - \alpha) \tag{27}$$

$$(D_3 + 1) U \cos(\omega^* t^* - \alpha) - D_4 U \sin(\omega^* t^* - \alpha) = Y \cos(\omega^* t^* - \beta) \tag{28}$$

with

$$D_1 = \frac{4\pi^2}{K_{\mathrm{FD}}}(K^* n^2 - M^* \eta^2), \quad D_2 = \frac{8\pi^2}{K_{\mathrm{FD}}\gamma}(K^* \zeta_B \eta n^2)$$

$$D_3 = \frac{4\pi^2}{K_{\mathrm{FD}}}(n^2 - \eta^2), \quad D_4 \frac{8\pi^2}{K_{\mathrm{FD}}}(\zeta_D \eta n^2) \tag{29}$$

Parameters ζ_B and ζ_D are the modal damping ratios[3] that are introduced for the base and the damper subsystems.

Alternatively, when the relative amplitude between the rods is sufficiently large to initiate slipping, the friction force at the base's first node is

$$F_f \approx \tilde{F}_f = \frac{K_{\mathrm{FD}}}{N}(F_c \cos\theta + F_s \sin\theta) \tag{30}$$

in terms of a one-term Fourier approximation, where $F_c = f_c/(k_t L) = R(\theta^* - 0.5 \sin 2\theta^*)/\pi$, and $F_s = f_s/(k_t L) = -4S(1 - S/R)/\pi$. By substituting Eqs. (22)–(25) and (30) into Eqs. (8) and (9), and by balancing the harmonic coefficients, the single algebraic equation that governs the relative motion R between the two rods becomes

$$(D_1 Y_c - D_2 Y_s - F_c)^2 + (D_1 Y_s + D_2 Y_c + F_s)^2 = \left(\frac{FK^*}{K_{\mathrm{FD}}}\right)^2 \tag{31}$$

in terms of the parameters

$$Y_c = \frac{F_s D_4 - F_c D_3}{D_3^2 + D_4^2} - R \quad \text{and} \quad Y_s = \frac{F_c D_4 + F_s D_3}{D_3^2 + D_4^2} \tag{32}$$

As the number of elements is increased relative to the excitation's wave number, the response amplitudes and phases of the base and damper as predicted by Eqs. (27), (28), and (31) become independent of N. Numerical solutions Y of the governing equations for finite N converge to the results for the limiting case $N/n \to \infty$. In that sense, the solution so obtained does not carry discretization error associated with the finite element treatment. Equations (27), (28), and (31) were also derived in [4] through the alternative approach of modeling the two-rod system as serial connections of frictionally coupled discrete springs and inertias, and the physical behavior of the system's response is described in detail there. The more general finite element method of Sec. 2 recovers the longitudinal vibration solution of [4] and is also applicable to other continuous structures as examined in Sec. 5.

5 Friction Damping of Transverse Bending Vibration

5.1 Vibration Model and Response. A ring damper can simultaneously damp in-plane and out-of-plane vibration of the base structure. Figure 7(*a*) depicts an assembly where the base is driven by a traveling wave force in the transverse direction. As in Fig. 7(*b*), vibration of the base/damper system is modeled in the first approximation by two beams having periodic boundary conditions that couple through friction. The transverse responses of the base structure and the damper at their first nodes are given by Eq. (15) following the analysis of Sec. 4. The flexural stiffness of the base (or damper) is taken as $k_{B(D)} = (EI)_{B(D)}/L^3$, where E is the elastic modulus and I is the second moment of area for the base or damper. The first natural frequency of the base (or damper) in the absence of contact is denoted $\Omega_{B(D)} = (2\pi)^2 \sqrt{k_{B(D)}/m_{B(D)}}$. For any integer value of n, frequency $\eta = n^2\gamma$ corresponds to the base structure's natural frequency in the absence of contact.

In terms of the cubic Hermite shape functions

$$\Phi_1(\xi) = 1 - 3\left(\frac{\xi}{L_e}\right)^2 + 2\left(\frac{\xi}{L_e}\right)^3, \quad \Phi_2(\xi) = \xi - 2\left(\frac{\xi^2}{L_e}\right)^2 + \xi\left(\frac{\xi}{L_e}\right)^2$$

[3]The proportional damping matrices for the base (B) and damper (D) are taken as $\mathbf{C}_{B(D)} = (2\zeta_{B(D)}/\Omega_{B(D)})\mathbf{K}_{B(D)}$, where Ω_B is the base's first flexible body natural frequency in the absence of contact. The modal damping ratios are taken illustratively as $\zeta_B = \zeta_D = 0.01\%$.

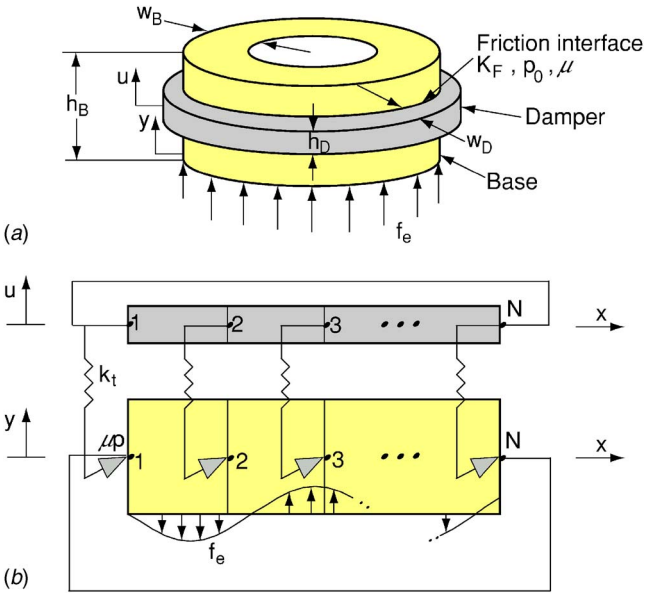

Fig. 7 (*a*) Base structure and ring damper systems that are subjected to transverse traveling wave excitation and (*b*) an idealized model comprising two unwrapped beams that have periodic boundary conditions and that couple through a spatially distributed friction interface. Parameters $w_{B(D)}$ and $h_{B(D)}$ denote the widths and heights of the base's and damper's cross sections, respectively.

$$\Phi_3(\xi) = 3\left(\frac{\xi}{L_e}\right)^2 - 2\left(\frac{\xi}{L_e}\right)^3, \quad \Phi_4(\xi) = \xi\left(\frac{\xi}{L_e}\right)^2 - \frac{\xi^2}{L_e}, \quad 0 \le \xi \le L_e \tag{33}$$

for a beam element with two nodal degrees of freedom [19], the elemental mass and stiffness matrices are

$$\mathbf{M}^e = \begin{bmatrix} 156 & 22L_e & 54 & -13L_e \\ 22L_e & 4L_e^2 & 13L_e & -3L_e^2 \\ 54 & 13L_e & 156 & -22L_e \\ -13L_e & -3L_e^2 & -22L_e & 4L_e^2 \end{bmatrix} \frac{\pi^2 M^* L_e}{105} \tag{34}$$

$$\mathbf{K}^e = \begin{bmatrix} 12 & 6L_e & -12 & 6L_e \\ 6L_e & 4L_e^2 & -6L_e & 2L_e^2 \\ -12 & -6L_e & 12 & -6L_e \\ 6L_e & 2L_e^2 & -6L_e & 4L_e^2 \end{bmatrix} \frac{K^*}{L_e^3} \tag{35}$$

For the ith element of the base structure, the kth entry of the excitation force vector is obtained from the projection

$$\mathbf{F}_k^e = e^{jw^* t^*}(FK^*) \int_0^{L_e} e^{-j2\pi n(x_i^* + \xi)} \Phi_k(\xi) d\xi \tag{36}$$

for $k = 1$, 2, 3, and 4. The global $\mathbf{M}_B$ and $\mathbf{K}_B$ reduce to two-by-two matrices after imposing condition (6), with $\mathbf{M}_D$ and $\mathbf{K}_D$ as given by Eq. (25).

The friction force that develops at each node acts in the transverse direction, so that the second entry of $\mathbf{F}_f$ vanishes regardless of whether the interface sticks, slips, or responds in some combination of the two. When the interface sticks, the friction force applied to the base's first node is identical to that in Eq. (26), and the base's and damper's responses are obtained by balancing exponential coefficients in Eqs. (8) and (9). In the general case with a combination of sticking and slipping, the friction force is represented by the complex form of the first term in a Fourier expansion as given by Eq. (18). The normalized friction force becomes

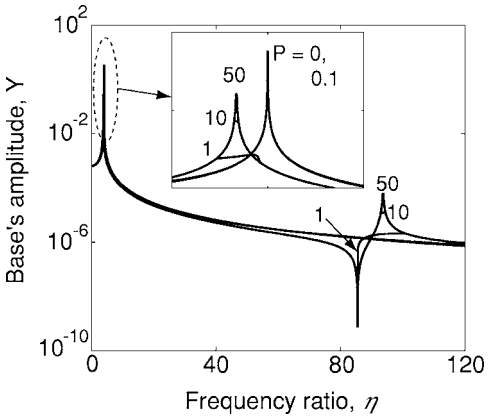

Fig. 8 Response of the base structure's amplitude for transverse bending vibration. The frequency responses are shown at five levels of preload; $M^*=5$, $L/h_D=33.3$, $\gamma=4$, $n=1$, $N=30$, and $F=1$.

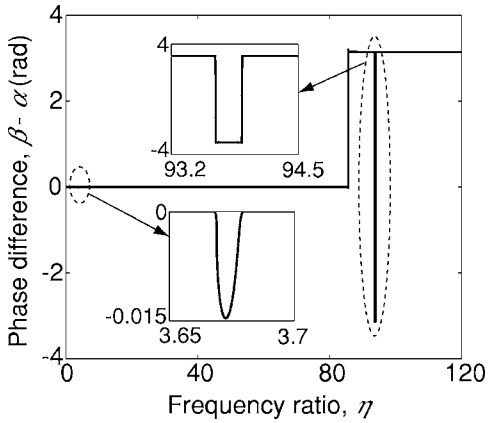

Fig. 9 Phase difference between the base's and damper's responses at $P=50$; other parameters are as specified in Fig. 8

$$\mathbf{F}_f \approx \tilde{\mathbf{F}}_f = \frac{K_{\mathrm{FD}}}{N}\left[F_{c1}e^{j\theta} + F_{-c1}e^{-j\theta}\ 0\right]^T \tag{37}$$

with $F_{c1}=(F_c-jF_s)/2$ and $F_{-c1}=(F_c+jF_s)/2$. The excitation at the base's first node is expressed in the similar form

$$\mathbf{F}_E = \mathbf{F}_{01}e^{j\theta} + \mathbf{F}_{-01}e^{-j\theta} \tag{38}$$

where the coefficients are found from $\mathbf{F}_E$ after assembly of the elemental force vectors at $i=1$ and N. The base's and damper's responses at the first node of each substructure then become

$$\mathbf{y} = \mathbf{b}_1 e^{j\theta} + \mathbf{b}_{-1}e^{-j\theta} \quad \text{and} \quad \mathbf{u} = \mathbf{g}_1 e^{j\theta} + \mathbf{g}_{-1}e^{-j\theta} \tag{39}$$

The response equation governing the interface's relative vibration amplitude R is then obtained by balancing the coefficients of $e^{j\theta}$ and $e^{-j\theta}$ in Eqs. (8) and (9). The base's response Y_{ND} when the damper is not present is obtained from Eq. (8) with the friction terms removed, and the maximum response value is denoted by $Y_{\mathrm{ND}}^{\max}$. The reduction in amplitude of the base's maximum response in the presence of friction is taken subsequently as a measure of the damper's performance and optimization.

5.2 Preload and Amplitude Reduction. The preload, and the relative mass and stiffness of the damper and the base, can, in principle, be tuned to maximize dissipation and attenuate the base structure's vibration. Figure 8 depicts the frequency response of the base's displacement at various levels of preload.[4] The base's maximum amplitude is most notably reduced at condition $P=1$ in Fig. 8. With the relatively low preload of 0.1, the response exhibits a single resonant peak near $\eta=4$, a frequency that corresponds to the base's natural frequency in the absence of contact. At that point, the base's motion is nearly undisturbed by the damper's presence. Likewise, when the preload is very high (for instance, at $P=50$), the damper is nearly pinned at the contact points, and the strongly coupled base/damper system behaves almost linearly as a monolithic structure with little or no relative motion occurring.

For the larger values of P, the growth in amplitude of the second resonant peak at $\eta\approx 95$ in Fig. 8 is representative of stronger dynamic coupling. As depicted in Fig. 9, the base and the damper vibrate out of phase relative to one another in the neighborhood of the second peak's resonance ($\eta\approx 95$) when $P=50$, but the two subsystems vibrate in phase at the lower frequencies. The small phase change near the first peak's frequency ($\eta\approx 4$), and the sudden phase change in the vicinity of the second peak's frequency, are manifestations of combined sticking and slipping at those frequencies.

The amplitude of relative vibration is compared in Fig. 10 with the interface's slip distance for the same choices of preload values as in Fig. 8. The regime $R/S>1$ denotes a combined sticking/slipping condition, while $R/S<1$ represents sticking and a linear motion that is dominated by interfacial stiffness. As the preload is gradually increased, the interface responds with slight slipping near the two peak frequencies only, and with pure sticking over an ever wider range of frequency in the vicinity of the lower resonances. For instance, at $\eta=n=1$, the condition that corresponds to the damper's natural frequency in the absence of contact, $R/S<1$ for all P. To the extent that no dissipation is then afforded to the base, the condition of integer η should be avoided in the damper's design and operation.

The results of Fig. 8 indicate that the contact pressure can be selected to minimize the base's response for a given frequency and amplitude of f_e. The base's maximal response $Y^{\max}$ with the damper attached is compared in Fig. 11 to $Y_{\mathrm{ND}}^{\max}$, the maximal response without the damper attached, as the preload is varied, and for several values of the mass ratio M^*. Under high preload, when $P>45$ and $M^*=100$, the base and damper couple in a nearly linear manner and the base's response is insensitive to preload. Should the damper become heavier or stiffer (or as M^* should decrease), the damper would become more effective in controlling the base's response and over a wider range of preload as well.

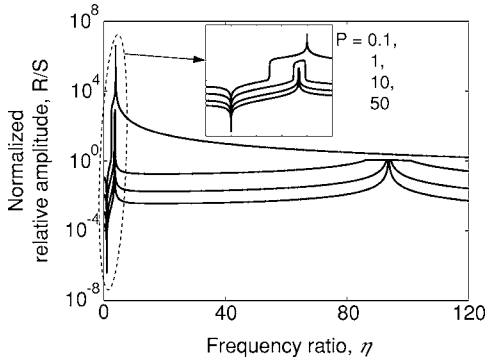

Fig. 10 Relative amplitude along the base/damper interface during transverse bending vibration. The frequency responses are shown at four levels of preload; other parameters are as specified in Fig. 8.

[4]The tangential stiffness of the interface is estimated by the shear expression $k_F=Gw_DL/(h_D/2)$, where G is the shear modulus of the damper's material. The stiffness ratio becomes $K_{\mathrm{FD}}=12(L/h_D)^4/(1+\nu)$, with the Poisson's ratio of the damper's material taken as $\nu=0.3$. In parameter studies of M^*, only w_D is considered to change, so that m_D and k_D vary with the same proportion.

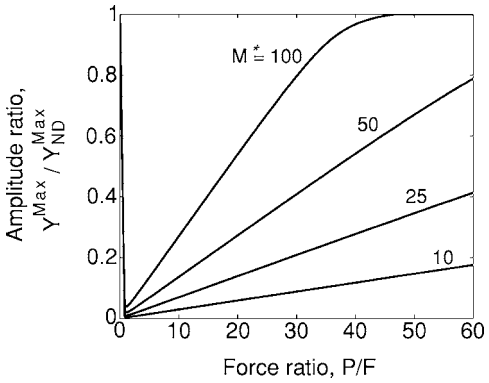

Fig. 11 Maximum amplitude of the base's motion when the damper is attached, under constant excitation amplitude, as normalized to the resonant amplitude of the base alone: $\gamma=4$, $L/h_D=33.3$, $n=1$, and $N=30$

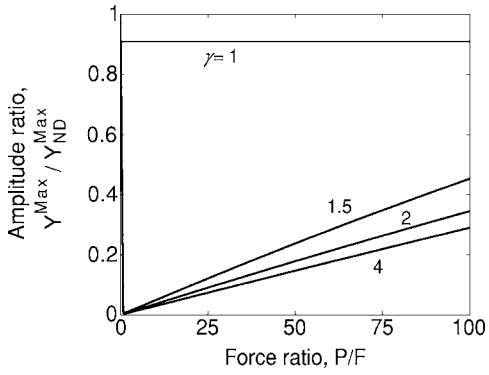

Fig. 12 Maximum amplitude of the base's motion when the damper is attached, under constant excitation amplitude, as normalized to the resonant amplitude of the base alone: $M^*=10$, $n=1$, $N=30$, and $L/h_D=8.3$, 12.5, 16.7, 33.3

5.3 Natural Frequency Ratio. The damper's performance over a range of preload also varies with the natural frequency ratio that exists between the base and damper subsystems in the absence of contact. Figure 12 depicts the manner in which $Y^{\max}$ changes relative to $Y^{\max}_{\mathrm{ND}}$ with respect to preload at different frequency ratios. In this case, the level of excitation is held constant and the preload is normalized relative to it.[5] The damper more effectively controls the base's response when the natural frequencies of the two subsystems are well-separated. In fact, the damper is least effective when $\gamma=1$, where little slippage develops when the two systems are excited at their common natural frequency. Such a damper design is preferentially avoided. The response of the system at $\gamma=1$ is dominated by the mass and stiffness of the combined base/damper system and therefore becomes insensitive to preload.

6 Summary

A finite element approach is described for the response of two axisymmetric structures that contact and couple through a spatially distributed hysteretic friction interface and that are subjected to traveling wave excitation. Owing to axisymmetry and the particular form of excitation, the steady-state responses of adjacent elements in the model are related by a phase shift and the dimension of the model's global mass and stiffness matrices can be reduced to the number of nodal degrees of freedom. This formulation offers significant analytical and computational advantages relative to alternative procedures that track the sticking and slipping states at all interfacial nodes during direct numerical simulation. Despite the presence of nonlinearity, and with contact occurring at an arbitrarily large number of interfacial nodal points, the response during sticking, or a combination of sticking and slipping, can be determined from a low-order set of computationally tractable nonlinear algebraic equations. In examples, the method is applied to prototypical systems of two rods that vibrate longitudinally and to two beams that vibrate transversely.

With the same natural frequency ratio (in the absence of contact) between the base and the damper, the damper's effectiveness for reducing the amplitude of the base's response is increasingly insensitive to variations in preload as the damper is made heavier or stiffer. The damper performs most effectively when its natural frequency is well below the base's natural frequency (in the absence of contact), and also when its natural frequency is well separated from the excitation frequency.

[5]With $E_{B(D)}$ being the elastic modulus, and $\rho_{B(D)}$ being the mass density of the base's (damper's) material, the natural frequency ratio becomes $\gamma=(h_B/h_D)\sqrt{E_B\rho_D/(E_D\rho_B)}$. For simplicity, the mass ratio M^* is held constant, and only h_D and w_D are varied to generate different γ values.

References

[1] Wickert, J. A., 2006, "Vibration of Disk Brake Rotors," *Disc Brake Squeal: Mechanism, Simulation, Test, and Prevention*, F. Chen, and C. A. Tan, eds., SAE International, Warrendale, PA.

[2] Wickert, J. A., and Akay, A., 1999, "Damper for Brake Noise Reduction," US Patent No. 5,855,257.

[3] Wickert, J. A., and Akay, A., 2000, "Damper for Brake Noise Reduction-Brake Drums," US Patent No. 6,112,865.

[4] Tangpong, X. W., Wickert, J. A., and Akay, A., 2006, "Distributed Friction Damping of Traveling Wave Vibration in Rods," Philos. Trans. R. Soc. London, in press.

[5] Griffin, J. H., 1980, "Friction Damping of Resonant Stresses in Gas Turbine Engine Airfoils," ASME J. Eng. Power, **102**, pp. 329–333.

[6] Menq, C. H., Griffin, J. H., and Bielak, J., 1986, "The Influence of a Variable Normal Load on the Forced Vibration of a Frictionally Damped Structure," ASME J. Eng. Gas Turbines Power, **108**, pp. 300–305.

[7] Lopez, I., Busturia, J. M., and Nijmeijer, H., 2004, "Energy Dissipation of a Friction Damper," J. Sound Vib., **278**(3), pp. 539–561.

[8] Tangpong, X. W., Karpenko, Y., Wickert, J. A., and Akay, A., 2005, "Optimizing Distributed-Contact Friction in Ring Dampers," *Proc. ASME International Design Engineering Technical Conference*, Long Beach, CA, ASME, New York, ASME Paper No. IDETC 2005-85066.

[9] Drago, R. J., and Brown, F. W., 1981, "The Analytical and Experimental Evaluation of Resonant Response in High-Speed, Lightweight, Highly Loaded Gearing," ASME J. Mech. Des., **103**(2), pp. 346–356.

[10] Lee, H. C., and Raider, J. W., 1979, "An Application of Beam Dynamics to a Damper Design," IBM J. Res. Dev., **23**(4), 386–391.

[11] Niemotka, M. A., and Ziegert, J. C., 1993, "Optimal Design of Split Ring Dampers for Gas Turbine Engines," *ASME International Gas Turbine and Aeroengine Congress Exposition*, Cincinnati, ASME Paper No. 93-GT-116.

[12] Wildheim, J., 1981, "Excitation of Rotating Circumferentially Periodic Structures," J. Sound Vib., **75**(3), pp. 397–416.

[13] Diaz, A. R., Haddow, A. G., and Ma, L., 2005, "Design of Band-Gap Grid Structure," Struct. Multidiscip. Optim., **29**, pp. 418–431.

[14] Thomas, D. L., 1974, "Standing Waves in Rotationally Periodic Structures," J. Sound Vib., **37**, pp. 288–290.

[15] Thomas, D. L., 1979, "Dynamics of Rotationally Periodic Structures," Int. J. Numer. Methods Eng., **14**, pp. 81–102.

[16] Caughey, T. K., 1960, "Sinusoidal Excitation of a System With Bilinear Hysteresis," ASME J. Appl. Mech., **27**, pp. 640–643.

[17] Berger, E. J., and Krousgrill, C. M., 2002, "On Friction Damping Modeling Using Bilinear Hysteresis Elements," ASME J. Vibr. Acoust., **124**, pp. 367–375.

[18] Song, Y., Hartwigsen, C. J., McFarland, D. M., Vakakis, A. F., and Bergman, L. A., 2004, "Simulation of Dynamics of Beam Structures With Bolted Joints Using Adjusted Iwan Beam Elements," J. Sound Vib., **273**, pp. 249–276.

[19] Becker, E. B., Carey, G. F., and Oden, J. T., 1981, *Finite Elements: An Introduction*, Prentice-Hall, Englewood Cliffs, NJ, Vol. 1.